Autonomous Sampling of Water Columns Using Gliding Robotic Fish: Algorithms and Harmful-Algae-Sampling Experiments

Feitian Zhang, *Member, IEEE*, Osama Ennasr, Elena Litchman, and Xiaobo Tan, *Senior Member, IEEE*

***Abstract*—Gliding robotic fish, which is a hybrid of underwater gliders and robotic fish, is energy efficient and highly maneuverable and holds strong promise for long-duration monitoring of underwater environments. In this paper, a novel scheme is proposed for autonomously sampling multiple water columns using gliding robotic fish. The scheme exploits energy-efficient spiral-down motion to sample each water column, followed by sagittal-plane glide-up toward the direction of the next water column. Once surfacing, the robot uses Global Positioning System guidance to reach the next column location through swimming. To enhance the path-tracking performance, a two-degree-of-freedom controller involving H_∞ control is used in the spiral motion, and a sliding-mode controller is employed to regulate the yaw angle during glide-up. The sampling scheme has been implemented on a gliding robotic fish prototype, "Grace," and verified first in pool experiments and then in field experiments involving the sampling of harmful algae concentration in the Wintergreen Lake, Michigan.**

***Index Terms*—Environmental monitoring, field robotics, nonlinear control system, underwater vehicles.**

I. Introduction

WATER resources and aquatic ecosystems around the world face increasing challenges and risks presented by natural and anthropogenic disasters, harmful algal blooms (HABs), global warming, and industrial and household waste discharges [1], [2]. Monitoring and understanding freshwater and marine environments enable informed decisions and, thus, hold the key to securing a sustainable future for water resources [3]. Among all sampling patterns, water column sampling is an important routine-surveying method in environmental studies. A water column is a conceptual narrow volume (similar to a narrow cylinder) of water stretching vertically from the surface to the bottom. Water column sampling allows the evaluation of the stratification or mixing of water layers and the examination of the variation of biophysical variables along the depth direction [4]–[6].

Existing approaches for water column sampling predominantly rely on humans operating a boat or a vessel and deploying the instrument on the spot, which is labor intensive and costly. Meanwhile, the use of robotic technology in aquatic environmental monitoring has made significant progress in the past decade [7]. Predominant examples of these technologies include remotely operated vehicles (ROVs) [8], autonomous surface vehicles (ASVs) [9], propeller-powered autonomous underwater vehicles (AUVs) [10], and underwater gliders [11]–[13]. ROVs typically have limited spatial access and autonomy due to their tethered nature, whereas the sampling space of ASVs is limited to the 2-D water surface. AUVs, on the other hand, can operate "freely" and autonomously in the 3-D water body, but their high price tags (upward of $150 K per vehicle) presents a huge barrier to their deployment in large numbers for high-resolution spatiotemporal coverage. While underwater gliders stand out in long-range missions with low energy consumption, they are relatively expensive and have poor performance in maneuverability. In the water column sampling task, underwater gliders typically require a turning radius of 30–50 m [12], which poses a significant limitation on the spatial sampling resolution, particularly for inland aquatic environments. Meanwhile, bioinspired robots have gained increasing scientific attention in the monitoring of aquatic environments [14], [15]. In particular, robotic fish [16]–[20], fish-like robots that achieve locomotion through oscillatory movement of body or fin devices, demonstrate excellent maneuverability. However, robotic fish require constant actuation to swim, which limits their operation time and, thus, sampling coverage per battery charge [21], [22].

As a hybrid of underwater glider [11]–[13] and robotic fish [16]–[20], a new type of underwater robots, i.e., gliding robotic fish, has been developed as an emerging platform for mobile sensing in aquatic environments [23]. Such a robot combines mechanisms of gliding and swimming and is thus both energy efficient and highly maneuverable. Similar to underwater gliders, a gliding robotic fish would realize most of its locomotion through gliding, by adjusting its buoyancy and center of gravity to enable motion without additional propulsion. On the other hand, it would use actively controlled fins to achieve high maneuverability, during turning and orientation maintenance. Of course, fins can also provide additional propulsive power

Manuscript received November 13, 2014; revised May 5, 2015; accepted May 21, 2015. Date of publication August 10, 2015; date of current version August 23, 2016. This work was supported by the National Science Foundation under Grant IIS 0916720, Grant IIS 1319602, Grant IIP 1343413, Grant CCF 1331852, and Grant ECCS 1446793. This work was conducted when Feitian Zhang was a Ph.D. student at Michigan State University.

F. Zhang is with the Department of Aerospace Engineering, University of Maryland, College Park, MD 20742 USA (e-mail: feitian.zhang@outlook.com).

O. Ennasr and X. Tan are with the Department of Electrical and Computer Engineering, Michigan State University, East Lansing, MI 48824-1226 USA (e-mail: ennasros@msu.edu; xbtan@msu.edu).

E. Litchman is with the Department of Zoology, Michigan State University, East Lansing, MI 48824 USA, and also with the W. K. Kellogg Biological Station, Michigan State University, Hickory Corners, MI 49060 USA (e-mail: litchman@msu.edu).

Digital Object Identifier 10.1109/JSYST.2015.2458173

during locomotion, if needed. A spiral motion of gliding robotic fish, which is produced when the robot glides with a deflected tail, has been studied in [22]. Due to its gliding nature, the spiral motion is energy efficient, and we have shown that the spiral radius can be as small as less than 1 m [22], thus providing high spatial resolution for the sampling. Due to its energy efficiency, tight spiral radius, and other desirable features, such as relatively small size, light weight, and low cost, the gliding robotic fish technology provides a promising solution to the water column-sampling mission.

In this paper, we propose a novel scheme for autonomously sampling multiple water columns based on the spiral motion of gliding robotic fish. The scheme exploits spiral-down motion to sample each water column, followed by sagittal-plane glide-up toward the direction of the next water column. The sagittal-plane gliding motion and the 3-D spiraling motion are utilized due to their great energy efficiency [21], [22]. Once surfacing, the robot uses Global Positioning System (GPS) guidance to reach the next column location through swimming.

Closed-loop control is applied to improve the path-following performance of the gliding robotic fish and, hence, the accuracy of the collected data. In particular, a two-degree-of-freedom (2-DOF) control strategy proposed in our prior work [24], involving an inverse feedforward controller and an H_∞ controller, is adopted to control the spiral motion. While only simulation results were presented in [24], a thorough investigation on the choice of sensor inputs, actuation outputs, and controller order is conducted in this paper, to obtain an effective H_∞ controller with the least implementation complexity. On the other hand, a sliding-mode controller developed in our earlier work for yaw angle stabilization [25] is adopted to maintain the desired orientation during glide-up. The effectiveness of the proposed sampling scheme is demonstrated with a gliding robotic fish prototype, first in pool experiments and then in field experiments at the Wintergreen Lake, Michigan, where the harmful algae distribution of 20 water columns is sampled. The collected data clearly indicate the spatial heterogeneity of the harmful algal concentration, along both the vertical and horizontal directions.

The remainder of this paper is organized as follows. We first present the design and implementation of the gliding robotic fish, including the actuation system, the electrical/electronic components and the mechanical system in Section II-A. Then in Section II-B, we review the dynamic model of the robot, followed by the discussion of its two energy-efficient working patterns, i.e., the steady glide and steady spiral, in Section II-C. The autonomous water-column-based sampling scheme is then proposed and discussed in Section III, followed by pool testing results in Section IV. The field test results on sampling harmful algae in Wintergreen Lake, Michigan, are presented in Section V. Finally, concluding remarks are provided in Section VI.

II. Gliding Robotic Fish

Here, the design and implementation of a fully functioning laboratory-developed gliding robotic fish prototype, named "Grace" (short for Gliding Robot ACE), are presented. The dynamic model of the robot is also reviewed along with the introduction of two energy-efficient locomotion modes, namely, rectilinear glide and gliding-based spiral.

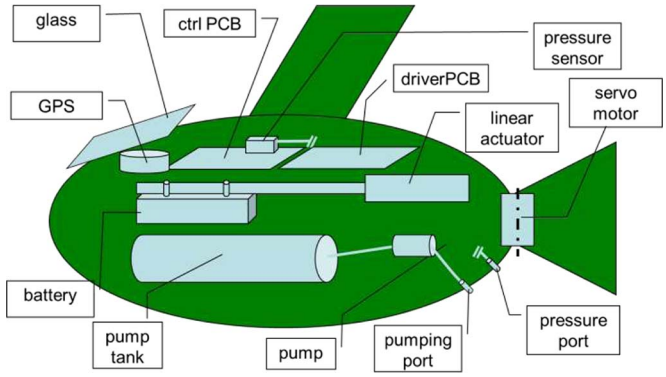

Fig. 1. Schematic of the internal configuration for "Grace" [25].

A. Design and Implementation

The gliding robotic fish "Grace" has three actuation systems for locomotion, namely, the buoyancy adjustment system, the center-of-gravity adjustment system, and the actively controlled tail system. The buoyancy adjustment system pumps water in and out of the robot's body to change the net buoyancy. When the robot weighs heavier than the fluid it displaces (negatively buoyant), the robot will descend; conversely, when it is lighter than the fluid it displaces (positively buoyant), the robot will ascend. The pumping is enabled by a heavy-duty linear actuator with integrated position feedback, which allows precise control of water volume despite the pressure differences at different depths. The center-of-gravity adjustment system uses another linear actuator to move a mass (battery pack) back and forth along a rail to change the center of the robot mass, for the purpose of controlling the pitch angle. The fish-like tail fin system of the robot is driven by a dc servo motor via a chain transmission. A deflected tail can be used in 3-D gliding to control the turning motion and heading direction. Similar to a real fish, "Grace" can also realize the swimming motion by flapping the tail.

A schematic of selected components for "Grace" is shown in Fig. 1. The components from three actuation systems can be identified. There are two physically separate printed circuit boards (PCBs). One is the *ctrl PCB* that contains the microcontroller and navigational sensors, including gyroscopes, accelerometers, and a digital compass; the other is the *driver PCB* that contains power regulators and actuator driver components for the linear actuators and the servo motor. A pressure sensor is employed to detect the depth of the robot. A GPS unit provides the position information and the universal time, when the robot is on the water surface.

Some other components are installed on the hull of the gliding robotic fish, including the wireless communication (Zigbee Pro) antenna, environmental sensors, and the GPS receiver, as shown in Fig. 2. "Grace" is equipped with a blue-green algae sensor and a temperature sensor. The sensor can be easily swapped to measure other environmental processes, such as

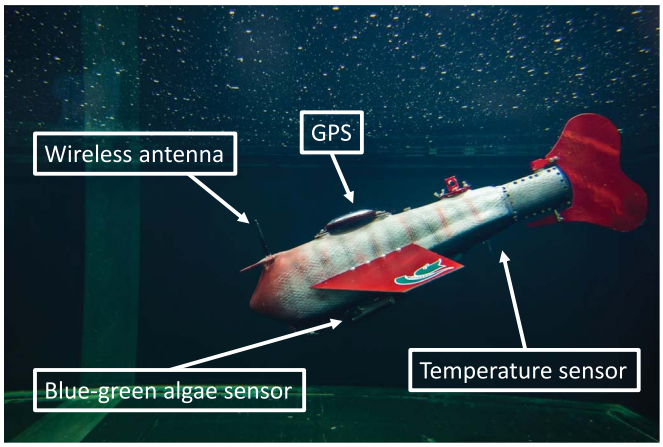

Fig. 2. Components equipped on the hull of "Grace."

TABLE I
SELECTED COMPONENTS USED IN "GRACE"

	Component name	Component model
1	Micro-controller	Microchip dsPIC6014A
2	Battery	Batteryspace 18.5V Polymer-Li-Ion battery
3	Linear actuator	Firgelli L16-140-63-12-P
4	Pump	Servocity 180 lbs thrust linear actuator
5	Servo motor	Hitec Servo HS-7980TH
6	Pressure sensor	Honeywell 40PC100G2A
7	GPS	Garmin GPS 18x LVC
8	Gyroscope	ST LPY503AL
9	Accelerometer+Compass	ST LSM303DLH
10	Wireless module	XBee Pro 900 XSC RPSMA
11	Wireless antenna	900MHz Duck Antenna RP-SMA
12	Algae sensor	Turner Designs Cyclops-7 Algae Sensor

chlorophyll, crude oil, turbidity, rhodamine, etc. Table I lists the details of the used components mentioned above.

We designed the mechanical system of the robot considering size, cost, and performance. The outer shell is made of lightweight and high-strength carbon fiber featuring a fish-like shape with a streamline profile to reduce drag. The robot is equipped with a pair of wings, made of aluminum sheets, to provide a hydrodynamic lift force that enables glide. The tail compartment is printed in composite polymer using a 3-D printer (Connex 350 from Objet). Some important physical parameters of "Grace" are as follows. Its length is 65 cm (body)/90 cm (total with tail), its width is 15 cm (body)/75 cm (total with wings included), and its height is 18 cm (body)/34 cm (total with antenna and sensor mounts). Its weight is 9 kg in total. The wings have trapezoidal shapes with a wingspan of 30 cm (one side) and an aspect ratio of 1.45. The tail with the servo compartment weighs 0.8 kg itself. The tail, as the only moving part seen from the outside, is detachable from the main body, for the purpose of easy service. The tail-flapping motion is obtained from the rotation of a servo through a chain system. Furthermore, the tail can be configured to flap sideways (similar to a shark) or up and down (similar to a whale).

Our gliding robotic fish as a hybrid of robotic fish and underwater gliders is unique in water-sampling applications. Robotic fish is generally developed for in-laboratory scientific research rather than for field deployment, whereas underwater gliders target oceanic environments. Underwater gliders are not suitable for shallow-water applications, such as in-land lakes, rivers, and even ponds, due to their high cost, energy consumption, and maintenance labor. Table II shows the comparison between gliding robotic fish and some underwater gliders in the literature, which suggests that our gliding robotic fish is a standout platform for shallow water-sampling missions with good balance between size and performance.

B. Dynamic Model

Here, we review the dynamic model for the gliding robotic fish, which serves as the basis for the controller design to be discussed later. The robot is modeled as a rigid-body system, holding an internal movable mass for center-of-gravity control and an internal water tank for buoyancy control. On the other hand, the deflected tail provides external thrust force, side force, and the yaw moment.

From our previous work [22], [25], the dynamic model for a gliding robotic fish can be described in the following equations:

$$\dot{\boldsymbol{b_i}} = \boldsymbol{R}\boldsymbol{v_b} \tag{1}$$

$$\dot{\boldsymbol{\Sigma}} = \boldsymbol{R_r}\boldsymbol{\omega_b} \tag{2}$$

$$\dot{\boldsymbol{v}}_{\boldsymbol{b}} = \boldsymbol{M}^{-1}(\boldsymbol{M}\boldsymbol{v_b} \times \boldsymbol{\omega_b} + m_0 g \boldsymbol{R}^{\boldsymbol{T}}\boldsymbol{k} + \boldsymbol{F_{ext}}) \tag{3}$$

$$\dot{\boldsymbol{\omega}}_{\boldsymbol{b}} = \boldsymbol{J}^{-1}\Big(- \dot{\boldsymbol{J}}\boldsymbol{\omega_b} + \boldsymbol{J}\boldsymbol{\omega_b} \times \boldsymbol{\omega_b} + \boldsymbol{M}\boldsymbol{v}_b \times \boldsymbol{v_b} + \boldsymbol{T_{ext}} + m_w g \boldsymbol{r_w} \times (\boldsymbol{R}^{\boldsymbol{T}}\boldsymbol{k}) + \bar{m} g \boldsymbol{r_p} \times (\boldsymbol{R}^{\boldsymbol{T}}\boldsymbol{k})\Big). \tag{4}$$

Here, the system states include the robot position $\boldsymbol{b_i} = (x\ y\ z)^T$, attitude $\boldsymbol{\Sigma} = (\phi\ \theta\ \psi)^T$, translational velocity $\boldsymbol{v_b} = (v_1\ v_2\ v_3)^T$, and angular velocity $\boldsymbol{\omega_b} = (\omega_1\ \omega_2\ \omega_3)^T$. $\boldsymbol{M}$ is the sum of the stationary mass matrix and added mass matrix; $\bar{m}$ is the movable mass with displacement $\boldsymbol{r_p}$ with respect to the origin O that is defined as the geometric center of the robot; m_w accounts for nonuniform hull mass distribution with displacement $\boldsymbol{r_w}$ with respect to the origin O, and m_0 is the excess mass, or the difference between the actual mass and mass of displaced water. $\boldsymbol{J}$ is the sum of the inertia matrix due to the stationary mass distribution and the added inertia matrix in water. $\boldsymbol{R}$, which is parameterized by three Euler angles included in Σ (roll angle ϕ, pitch angle θ, and yaw angle ψ), represents the rotation matrix from the body-fixed reference frame to the inertial frame, and matrix $\boldsymbol{R_r}$ represents the relationship between the angular velocity in the body-fixed frame and the Euler angle changing rate. In addition, g is the gravitational acceleration, $\boldsymbol{k}$ is the unit vector along the gravity direction in the inertial frame, $\boldsymbol{r_w}$ is a constant vector, and $\boldsymbol{r_p}$ is the controllable movable mass position vector, which has one degree of freedom in the longitudinal direction. $\boldsymbol{F_{ext}}$ stands for all external forces: the external thrust force $\boldsymbol{F_t}$ induced by tail flapping and the external hydrodynamic forces (lift force L, drag force D, and side force F_S) acting on the gliding robotic fish body, expressed in the body-fixed frame. Finally, $\boldsymbol{T_{ext}}$ is the total hydrodynamic moment caused by $\boldsymbol{F_{ext}}$. The hydrodynamic forces and moments are dependent on the angle of attack α, the sideslip angle β, the velocity magnitude V, and the tail angle δ.

TABLE II
COMPARISON OF OUR GLIDING ROBOTIC FISH "GRACE" WITH OTHER UNDERWATER GLIDERS REPORTED IN THE LITERATURE. VELOCITY REFERS TO THE TERMINAL VELOCITY

Name	Manufacturer	Length	Weight	NetBuoyancy	Velocity
Slocum Glider [26]	Teledyne Webb Research	1.5 m	52 kg	450 g	0.4m/s
Spray Glider [26]	Bluefin Robotics	2.0 m	51 kg	900 g	0.45 m/s
Seaglider [26]	iRobot	1.8 m	52 kg	840 g	0.45 m/s
ANT Littoral Glider [27]	ANT, LLC	2 m	120 kg	–	1.03 m/s
ALBAC Glider [27]	University of Tokyo	1.4 m	45 kg	–	0.51 m/s
Autosub LR [28]	UK National Oceanography Center	–	650 kg	2 kg	0.42 m/s
Odyssey [27]	MIT	2.6 m	650 kg	–	1.54 m/s
Gliding robotic fish "Grace"	Michigan State University	0.9 m	9 kg	100 g	0.2 m/s

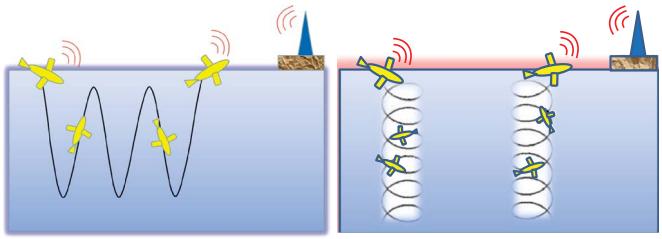

Fig. 3. Schematics of two energy-efficient working patterns for gliding robotic fish. (a) Gliding in sagittal plane. (b) Spiraling in 3-D space.

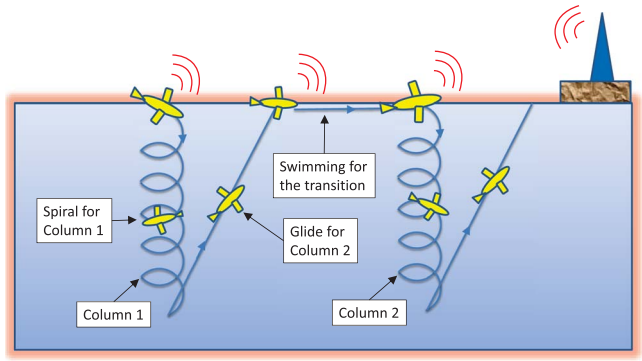

Fig. 4. Schematic of the autonomous water-column-based sampling scheme using spiraling and gliding motions.

C. Steady-State Locomotion Modes

Here, we review two energy-efficient working patterns of gliding robotic fish, i.e., the steady glide and the steady spiral. The steady glide [see Fig. 3(a)] is also the predominant operating mode for traditional underwater gliders. In the zigzag trajectory, the buoyancy-driven gliding robotic fish only consumes energy during the transitions between descent and ascent, which makes it energy efficient.

The other motion, i.e., steady spiral [see Fig. 3(b)] in 3-D space, is achieved by gliding with the fish-like tail deflected [22]. The deflected tail fin introduces a steering moment and leads to a 3-D spiraling motion. With the actively controlled tail, the gliding robotic fish is capable of spiral motions with a turning radius as tight as 1 m, significantly increasing the sampling resolution, in comparison with the spiral by traditional underwater gliders (a typical radius is 30–50 m [12], [29]).

Ideally, a gliding robotic fish holds a preset steady gliding path (steady rectilinear glide or spiral) for most of its operation time. However, the robot is subjected to many nonnegligible disturbances from the aquatic environment (e.g., waves and currents), which could push the robot off its desired trajectory. Consequently, feedback control of the gliding and spiraling motions is of practical interest, and the implementation and integration of such control strategies to realize autonomous water column sampling are a primary focus of this paper.

III. AUTONOMOUS SAMPLING SCHEME FOR MULTIPLE WATER COLUMNS

Here, a systematic autonomous water-column-based sampling scheme is proposed for gliding robotic fish. First, 3-D spiral and sagittal-plane glide are adopted and integrated in path planning to achieve energy-efficient operation for the major part of the sampling mission. A GPS-based guidance law is further designed to drive the robot to the next water column targets via surface swimming. To enhance the path-following performances for underwater sampling, closed-loop control for spiral motion stabilization and glide heading regulation is implemented.

A. Overview of the Sampling Scheme

As discussed in Section II-C, the spiral motion is a suitable method for sampling a water column. In this paper, we consider autonomous sequential multiple-water-column sampling for covering a large area of water body. For each water column, a feedback-controlled steady spiral motion is proposed to collect the vertically distributed water quality data. For the transition between neighboring water columns, a steady rectilinear glide motion is proposed, with a feedback-controlled heading direction that points to the next target column. As shown in Fig. 4, the robot spirals down in the first water column while collecting data in that column and then switches to the sagittal-plane glide mode at the bottom of the spiral to transition toward the next water column. When the robot glides up to the water surface, it usually will not be at the target column yet, due to environmental disturbances or other factors (e.g., the separation between the water columns could be greater than the horizontal travel achievable during the glide-up). Therefore, a tail-flapping swimming mode is applied with GPS-aided guidance, to drive the robot to the target column location.

B. Closed-Loop Controllers for Autonomous Sampling

Due to various disturbances in the underwater environment, closed-loop control is desired and necessary for keeping the

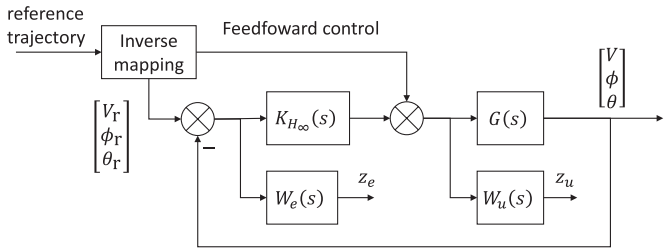

Fig. 5. Diagram for the proposed 2-DOF control system.

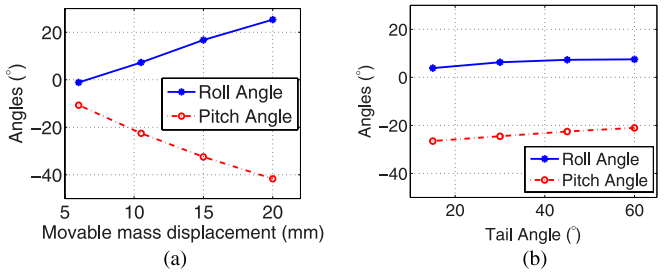

Fig. 6. Influence of different actuators on the steady-state pitch angle and the roll angle during spiraling. (a) Impact of the movable mass displacement, where the tail angle is fixed at 45°. (b) Impact of the tail angle, where the displacement is fixed at 10.5 mm.

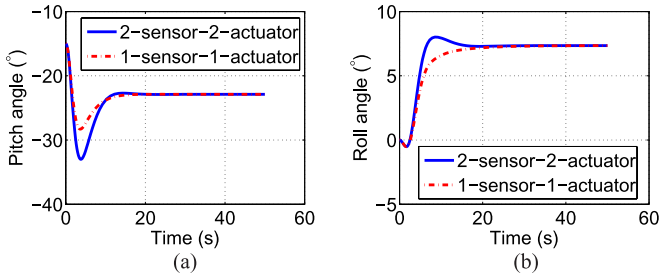

Fig. 7. Comparison between the two-input–two-output control and the single-input–single-output control. (a) Trajectory of pitch angle. (b) Trajectory of roll angle.

robot close to the designed path, so that the collected data are better correlated with their spatial locations—since it is difficult to obtain a precise horizontal location when the robot is underwater, better tracking of a planned trajectory helps alleviate the data association problem. In the following, we describe the three controllers used for spiral control, rectilinear glide control, and swimming control, at different phases of the sampling scheme. While intelligent control approaches, such as fuzzy logic controllers, could be potentially applied in our application, we have chosen to focus on model-based nonlinear control methods that do not rely on human expertise in the specific application domain.

1) Spiral Control: As studied with simulation in our previous work [24], a 2-DOF controller stabilizes the spiral motion and leads to quick convergence in the presence of environmental disturbances. The 2-DOF controller consists of a feedforward controller using static inverse mapping and a feedback controller using H_∞ control design, as shown in Fig. 5. The feedforward controller enables the system to operate around the desired equilibrium, and the feedback controller enhances the tracking performance. In the control system diagram, $G(s)$ is the transfer function for the system plant, and $K_{H_\infty}(s)$ is the transfer function of the feedback controller using H_∞ analysis. $K_{H_\infty}(s)$ is designed using weighting function $W_e(s)$ and $W_u(s)$ such that the H_∞ norm of the transfer function from the vector signal $(V, \phi, \theta)^T(s)$ to the weighted signal (z_e, z_u) is minimized. In particular, the H_∞ controller requires three sensor measurements (velocity V, roll angle ϕ, and pitch angle θ) and three actuation inputs (net buoyancy m_0, tail angle δ, and displacement of movable mass r_p). The designed H_∞ controller can be expressed in a compact form in the following equation:

$$(m_0, \delta, r_p)^T(s) = K_{H_\infty}(s)(V,\ \phi,\ \theta)^T(s). \tag{5}$$

The controller performance is satisfactory as shown in simulation; however, it is not feasible to fully implement such a controller on the gliding robotic fish prototype. For example, the velocity information is not available from the sensors on "Grace," which is a common case and a challenge for such low-speed underwater robots; on the other hand, the net buoyancy control requires significant energy consumption compared with other actuator controls, and the bandwidth of buoyancy control is low (due to limited pumping speed). Moreover, the designed H_∞ controller $K_{H_\infty}(s)$ has a high order of ten. It is not practical to implement such a controller in the microcontroller due to the computational burden and the resulting accumulated computational error caused by sensor noise.

In this paper, we propose a more practical H_∞ controller with reduced order for the stabilization of spiral motion. Through simulation, we choose a second-order single-input–single-output H_∞ controller, which achieves similar performance as the original tenth-order three-input–three-output controller. The justification of the controller simplification is as follows.

First, as explained above, the net buoyancy adjustment should be avoided in feedback control due to energy consumption concerns, and the velocity information is not available for feedback. Simulation has been performed to further facilitate the choice of actuation inputs. As shown in each subfigure in Fig. 6, we fix one actuation input and compute the steady-state values of roll and pitch angles under a step change of the other actuation input to different values. The results indicate that the influence of the tail angle on the roll and pitch angles is much smaller than that of the movable mass displacement (note that there is no steady-state value for the yaw angle since it is constantly varying during spiral), which suggests that the controller could function adequately well using only one actuator (movable mass displacement). Furthermore, Fig. 7 shows the comparison on the trajectories of the pitch angle and the roll angle between using a single-input–single-output controller and using a two-input–two-output controller. Here, the single-input–single-output controller uses pitch angle as the only sensor measurement and the movable mass displacement as the only actuator output. The simulation results show that the performance of the single-input–single-output controller is comparable to that of the two-input–two-output controller. In particular, the single-input–single-output controller has slightly longer convergence time but has less overshoot. We have also investigated the impact of reduced controller order. Specifically,

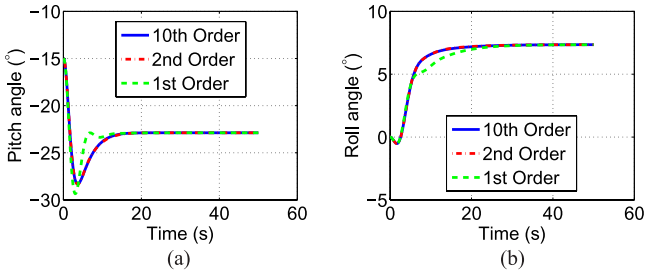

Fig. 8. Comparison between controllers with different orders. (a) Trajectory of pitch angle. (b) Trajectory of roll angle.

we use a Hankel singular-value-based model reduction method to obtain controllers with reduced orders from the original tenth-order H_∞ controller. Fig. 8 shows the simulation results of the pitch angle and the roll angle when using controllers with different orders in spiral stabilization, which shows that the second-order controller still provides satisfactory stabilization performance that is close to that of a full-order controller, whereas a first-order controller would result in largely degraded performance.

Based on the above discussions, a second-order single-input–single-output H_∞ controller is adopted in this paper for spiral motion stabilization and further applied in the field test in Section V. The specific controller used in this paper for "Grace" is given below as implemented in discrete time, i.e.,

$$r_p(k) = 0.968\, r_p(k-1) - 0.06094\, \Delta\theta(k-1) + 0.06015\, \Delta\theta(k-2). \quad (6)$$

Here, $\Delta\theta(k)$ represents the difference of the pitch angle from its equilibrium point value at the kth time step.

2) Rectilinear Gliding Control: In the glide motion part, a sliding-mode controller is used to regulate the yaw angle and, hence, the heading direction of the robot. The desired yaw angle ψ_e is calculated based on the GPS coordinates of the two neighboring water columns. As reported in [25], the sliding-mode controller is able to provide a robust orientation-maintaining performance for the nonlinear dynamics of gliding robotic fish. This controller requires only the yaw angle measurement ψ and tail angle control δ, which is easy to implement on the robot. The controller is realized as

$$\delta = -\left(k_1 \|\psi - \psi_e\|_2^{k_2} + k_3\right) \mathrm{sat}\left(\frac{s}{\epsilon}\right). \quad (7)$$

Here, $s = (\dot{\psi} - \dot{\psi}_e) + k_0(\psi - \psi_e)$ is the sliding manifold, and the dot notation $\dot{\psi}$ stands for the time derivative operation; $\mathrm{sat}(\cdot)$ is a high-slope saturation function with a small-valued constant ϵ to reduce chattering. The constants k_0, k_1, k_2, and k_3 are controller parameters to tune the balance between control effort and convergence speed and the balance between the steady-state heading orientation error and the disturbance rejection performance.

3) Swimming Control: After the robot surfaces, it will first send the data back to the base station or simply store the data in the on-board memory and then use the GPS information to navigate to the next sampling target. In this paper, the guided swimming is realized using a proportional controller with the tail flapping bias θ_{bias} as the control variable, which is designed to be proportional to the angle error between the target direction ψ_{target} and the velocity direction ψ_{velocity}, i.e.,

$$\theta_{\mathrm{bias}} = K_{\mathrm{bias}}(\psi_{\mathrm{target}} - \psi_{\mathrm{velocity}}). \quad (8)$$

The velocity direction is computed using the difference between the current GPS coordinates and those at the previous time step; the time step for this calculation is set to be 5 s, to accommodate the error of the GPS reading. The compass is not used here because first, it represents the body orientation but not the velocity direction, and second, due to the swimming motion, the body orientation constantly oscillates.

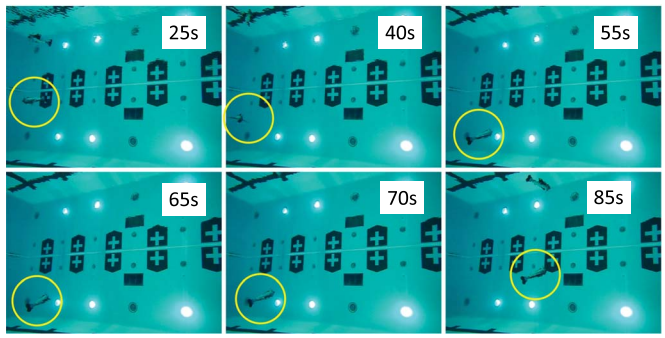

Fig. 9. Snapshots of "Grace" in the column-switching test in an indoor pool at Michigan State University. The one in the yellow circles was the real robot, whereas the other object above it was its reflection from the water surface.

IV. Experimental Results in Swimming Pools

The autonomous sampling scheme was implemented, tuned, and tested in both indoor and outdoor swimming pools at Michigan State University before the field tests were conducted.[1] Fig. 9 shows the snapshots of the column-switching test conducted in an indoor pool. Before 55 s, "Grace" performs a controlled spiral to sample the water column. At 55 s, the robot performs the transition and switches to the rectilinear glide motion guided by the sliding-mode controller toward the next water column (after 65 s). Fig. 10 shows the trajectories of the system variables during the column-switching motion. During the spiral motion (before 55 s), the yaw angle linearly changes with time as expected [see Fig. 10(a)], whereas the pitch angle [see Fig. 10(b)] and the roll angle [see Fig. 10(c)] are stabilized to their equilibrium values via H_∞ control with movable mass displacement as the actuation input [see Fig. 10(e)]. During the rectilinear glide motion (after 70 s), the yaw angle is regulated to the preset value of 100° [see Fig. 10(a)] with sliding-mode control using the tail angle as the actuation input [see Fig. 10(f)]. Fig. 11 shows the trajectory of the robot when tested in the outdoor pool for the surface-swimming navigation algorithm. The blue pin is the location where "Grace" started to dive, and the red pin is the location where the robot surfaced. The yellow pins show the trajectory when the robot swam back to the dive point for the repeated water column sampling at the same location.

[1] Visit our youtube site at http://youtu.be/pgidFJT3iRE and http://youtu.be/gIRySLGIjqY for short demo videos.

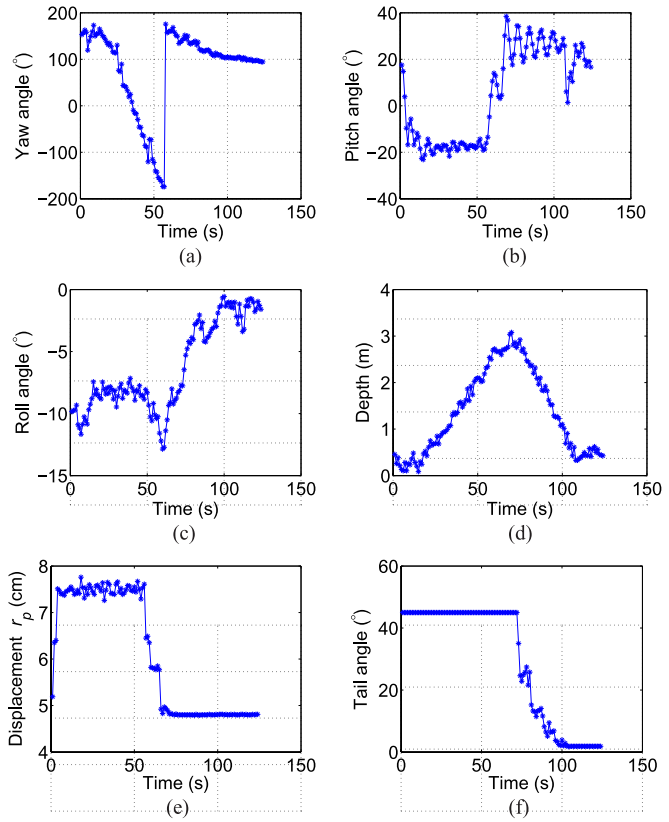

Fig. 10. Trajectories of the system variables for the indoor pool test. (a) Yaw angle. (b) Pitch angle. (c) Roll angle. (d) Depth. (e) Movable mass displacement. (f) Tail angle.

Fig. 11. GPS trajectory of "Grace" in the water-surface swim control test in IM West outdoor pool at Michigan State University.

V. Field Test Results in Wintergreen Lake

The proposed water-sampling scheme was tested in Wintergreen Lake, Michigan, using the gliding robotic fish prototype "Grace" (see Fig. 12). Wintergreen Lake has a surface area of 164 000 m^2. The maximum depth is 7.9 m, and the mean depth is 2.4 m. In the field test,[2] a blue-green-algae sensor was used to measure the concentration of harmful algae. HABs [30] deteriorate water bodies by producing potent toxins that can

[2]Visit our youtube site http://youtu.be/7ybtkn1cdHs for a short demo video of the field test.

Fig. 12. "Grace" swimming in the field test in Wintergreen Lake, Michigan.

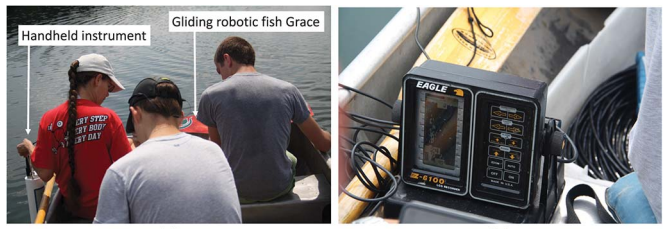

Fig. 13. Sensor calibration and depth surveying. (a) Handheld HydroLab instrument for algae concentration. (b) Depth meter EAGLE Z-6100.

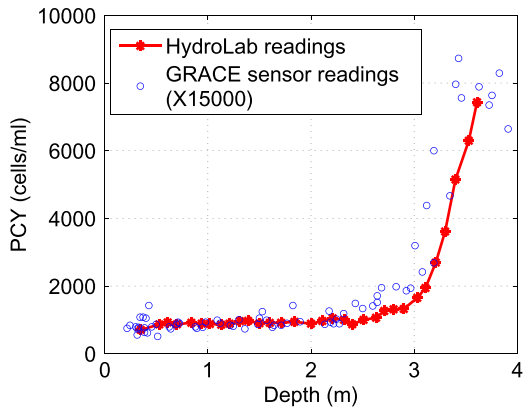

Fig. 14. "Grace" algae sensor reading, sampled in one water column, calibrated with HydroLab reading.

get into water supplies and present health hazard. Excessive growth of harmful algae (cyanobacteria) also results in decaying biomass and oxygen depletion, which are harmful to fish and other aquatic life.

Calibration of the on-board algae sensor was first carried out using an handheld instrument, namely, HydroLab sonde [see Fig. 13(a)], in a single water column. The HydroLab instrument was manually lowered to different depths when the boat was securely anchored. The device needs to stay at each depth for at least 10 s to take algae measurement. Meanwhile, the gliding robotic fish "Grace" was commanded to perform a spiral motion at the same location to sample the water column. A gain parameter that relates the onboard sensor reading to the

Fig. 15. Illustration of GPS coordinates for the sampled points and desired targets in Wintergreen Lake. The yellow pins are the designed 20 water-column targets in a 4-by-5 grid, and the blue pins are the actual sampling water-column points in the field test.

algae cell counts per volume was identified offline using curve-fitting techniques, as shown in Fig. 14. The result shows a satisfactory match in the trend of algae distribution with respect to depth between the on-board algae sensor and the HydroLab Sonde instrument. With a depth meter [see Fig. 13(b)], we scouted out a region that had a minimum depth clearance of 5 m. A 4-by-5 sampling grid with 20 target water columns was selected inside the safe sampling area represented by the yellow pins in Fig. 15. The separation between neighboring water columns was approximately 20 m, which was chosen based on the typical spatial scale of HAB dynamics [5], [6]. Each water column has a diameter of 1 m. In the experiment, the dive depth was set to be 3.5 m.

A graphical user interface was created for the base station (a laptop in this work), which uses an XBee Pro 900 unit to send commands to and receive data from "Grace." A sequence of target water-column GPS coordinates and desired heading directions for column switching are loaded into the software as a.TXT file and then sent to "Grace" as the sampling operation progresses.

Blue pins in Fig. 15 represent the actually sampled water-column points, whereas the yellow pins represent their desired locations. The positioning error is approximately 3 m, which is determined by the GPS resolution. On average, the sampling of each column took about 5 min, including the spiral-down, glide-up, data transmission, and swimming to the next column. Since the time scale of harmful algae growth dynamics is on the order of 0.5–1 day [5], [6], one can consider that all 20 columns were sampled at the same time instant. As an example, Figs. 16 and 17 show the trajectories of some system states and the sensor measurements in the sampling of one column (column #19). From 0 to 60 s, the yaw angle changes at an approximately constant rate, whereas the pitch angle and the roll angle are kept almost constant (see Fig. 16), which are characteristic of the spiral motion. During this period, the movable mass displacement is used as the actuator to stabilize the spiral with a 2-DOF controller, whereas the tail is kept at a constant deflected angle (see Fig. 17). From 60 to 125 s, the robot pumps water out and transitions to the glide-up mode. The yaw is controlled

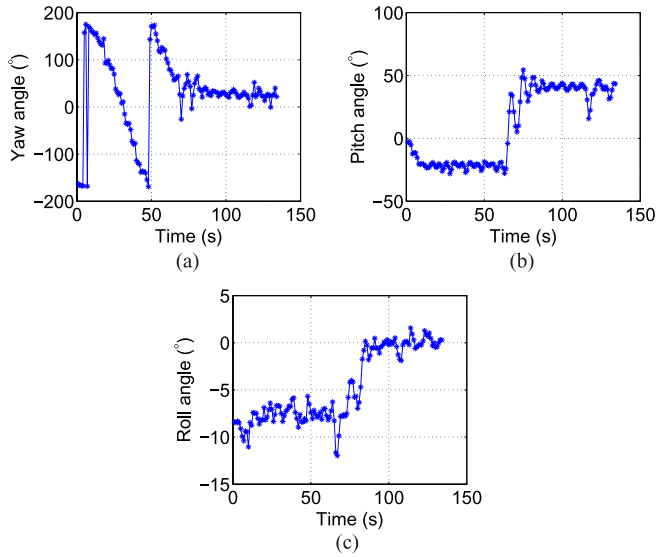

Fig. 16. Trajectories of the robot system states for the 19th sampled water column. (a) Yaw angle. (b) Pitch angle. (c) Roll angle.

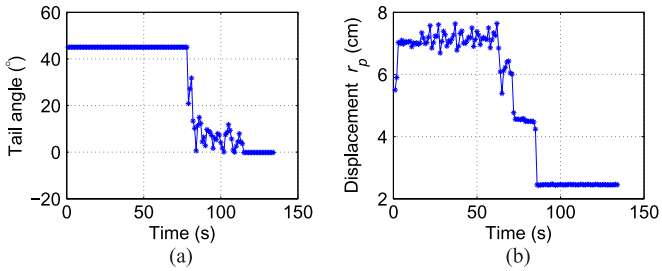

Fig. 17. Trajectories of the system actuator outputs for the 19th sampled water column. (a) Tail angle. (b) Movable mass displacement.

to the desired direction that points to the next water column target (see Fig. 16), when the sliding-mode controller utilizes only the tail angle for orientation regulation (see Fig. 17). The system dynamics in the field test matches the one in the pool experiments (see Fig. 10), which shows the consistency of the system behavior in different environments.

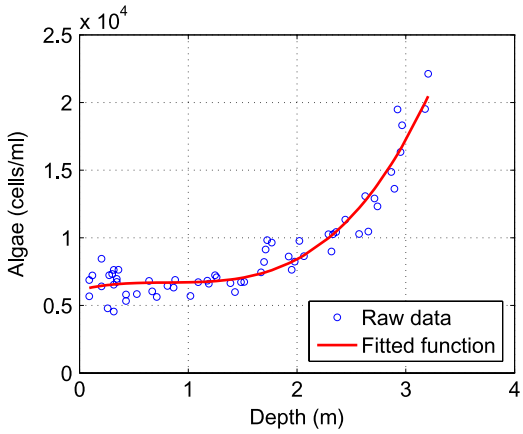

Fig. 18. Algae concentration PCY (cells/ml) with respect to the depth for the first sampled water column.

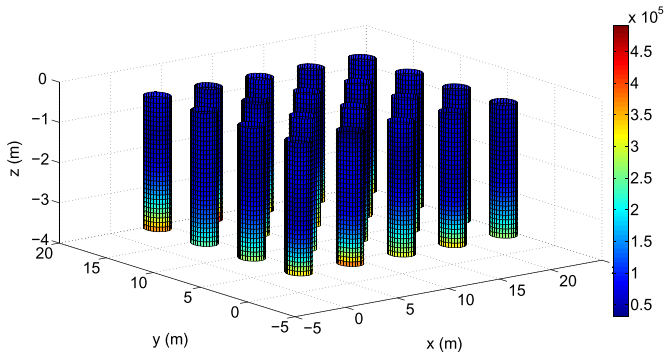

Fig. 19. Algae concentration distribution PCY (cells/ml) for the sampled 20 water columns. The separation between columns is artificially set to 5 m rather than 20 m for a better display.

Fig. 18 shows the algae concentration with respect to the depth in the first sampled water column. To smoothen the raw data (represented by blue circles) and get an analytical expression of the algae concentration, we adopt a third-order polynomial to fit the sampled data (represented by a red solid line). Here, we assume that the algae concentration is constant at each depth within the sampled column, whose diameter is about 1 m, which is estimated with simulation. Fig. 19 shows a visualization of the algae density in all 20 sampled water columns. While the quantitative implications of the data are still under analysis, some key observations can be drawn from the figure. In particular, the algae concentration shows pronounced spatial heterogeneity along the depth direction. This is consistent with the general understanding of algal dynamics, since the water in the deeper region is more stagnant, which facilitates algae growth. On the other hand, the data clearly show variation across the water columns (see, for example, the concentrations at the bottom of each water column as shown in Fig. 20). While such variations along the horizontal directions have been suspected by ecologists, the relevant data available are scarce, primarily due to the difficulty with existing methods in sampling water columns at adequate resolutions. Therefore, our field tests have demonstrated the promise of gliding robotic fish in filling this important void in the current sampling practice.

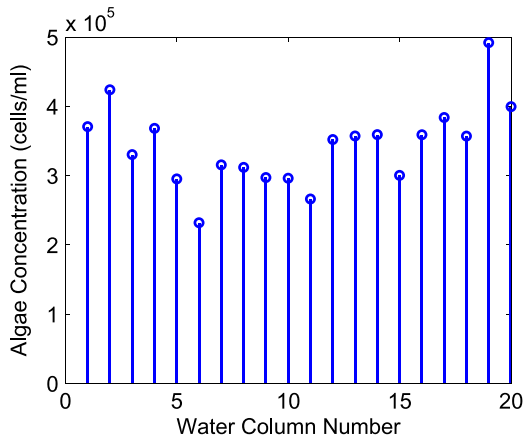

Fig. 20. Algae concentration (cells/ml) at the bottom of each water column with a depth of 3.5 m.

The environmental data gathered by "Grace" included both cyanobacteria concentration and temperature, although only the cyanobacteria concentration data were discussed in the interest of brevity. As a sensor platform, gliding robotic fish can be equipped with a multitude of *in situ* sensors to provide simultaneous measurement of multiple biophysical variables. For example, another prototype under development will be equipped with sensors to simultaneously measure cyanobacteria, chlorophyll, temperature, dissolved oxygen, and photosynthetically active radiation. Such data will be directly instrumental not only in monitoring but also in facilitating mechanistic modeling and, thus, fundamental understanding of aquatic processes, such as the development of HABs. The measurement data and the scientific understanding developed from the data are essential to environmental assessment and water resource management [31]. For example, high-density cyanobacterial algae in water leads to various human health risks [32] through direct exposure and food chain and could possibly cause an unpredictable long-term impact on ecosystems [33], [34]. Thus, the information that gliding robotic fish is able to provide helps in environmental decision-making for maintaining healthy and balanced aquatic ecosystems.

VI. Conclusion and Future Work

In this paper, we have proposed a novel approach to autonomous sampling of multiple water columns using gliding robotic fish. First, the gliding robotic fish was introduced and discussed in terms of its design, implementation, dynamic model, and two energy-efficient motions (sagittal-plane glide and 3-D spiral). Then, we proposed a systematic autonomous sampling scheme, which integrates two energy-efficient gliding motions and surface swimming. Closed-loop control was implemented onboard to facilitate path-following. Finally, we presented the field test results in Wintergreen Lake, Michigan, to demonstrate the effectiveness of the proposed autonomous sampling scheme.

While robotics has played an increasingly important role in aquatic environmental research, the field still faces several critical challenges that limit the application of robotic technology, which include autonomy in uncertain and spatially and

temporally varying environments with limited communications, rapid and dynamic responses to user needs, and cooperation among heterogeneous platforms, to name a few [35]. The development of gliding robotic fish provides a new platform for studying and tackling those problems.

We note that while the feedback control in the spiral-down motion helps maintain some system states at their desired values, it does not ensure that the robot stays within the desired column under external disturbances (for example, lateral current disturbances). Therefore, as part of our future work, we will investigate the use of underwater localization techniques to achieve better assurance of column-keeping. In addition, in this paper, we assume that the target water columns are given *a priori*. In the absence of additional information, this would mean that the columns will be uniformly distributed. Our ongoing research involves the exploration of a more efficient adaptive sampling approach, where the next water column location is determined based on the data collected so far, to maximize the information gain from the next water column.

ACKNOWLEDGMENT

The authors would like to thank J. Thon, C. Thon, P. Woodruff, and K. Shchapov for their help in preparing and conducting the field test in Wintergreen Lake, Michigan.

REFERENCES

[1] NOAA Office of Response and Restoration. NOAA Deepwater Horizon/BP Oil Spill Archive. [Online]. Available: http://response.restoration.noaa.gov/deepwaterhorizon

[2] B. C. Bates, Z. Kundzewicz, S. Wu, and J. Palutikof, Eds., *Climate Change and Water*. Geneva, Switzerland: Intergovernmental Panel Climate Change, IPCC Secretariat, 2008.

[3] J. Bartram and R. Ballance, Eds., *Water Quality Monitoring: A Practical Guide to the Design and Implementation of Freshwater Quality Studies and Monitoring Programmes*. London, U.K.: E & FN Spon, 1996.

[4] M. Schwartz, *Encyclopedia of Coastal Science*, vol. 24. Norwell, MA, USA: Kluwer, 2005.

[5] J. P. Mellard, K. Yoshiyama, E. Litchman, and C. A. Klausmeier, "The vertical distribution of phytoplankton in stratified water columns," *J. Theoret. Biol.*, vol. 269, no. 1, pp. 16–30, Jan. 2011.

[6] C. A. Klausmeier and E. Litchman, "Algal games: The vertical distribution of phytoplankton in poorly mixed water columns," *Limnol. Oceanogr.*, vol. 46, no. 8, pp. 1998–2007, Nov. 2001.

[7] M. Dunbabin and L. Marques, "Robotics for environmental monitoring," *IEEE Robot. Automat. Mag.*, vol. 19, no. 1, pp. 24–39, Mar. 2012.

[8] A. Goldstein and S. Bentley, "Use of highly portable micro-sized remotely operated vehicles for environmental monitoring and mapping," in *Proc. OCEANS Conf.*, Seattle, WA, USA, 2010, pp. 1–6.

[9] G. Hitz *et al.*, "Autonomous inland water monitoring: Design and application of a surface vehicle," *IEEE Robot. Automat. Mag*, vol. 19, no. 1, pp. 62–72, Mar. 2012.

[10] L. L. Whitcomb *et al.*, "Navigation and control of the Nereus hybrid underwater vehicle for global ocean science to 10,903 m depth: Preliminary results," in *Proc. IEEE Int. Conf. Robot. Autom.*, Anchorage, AK, USA, 2010, 594–600.

[11] O. Schofield *et al.*, "Slocum gliders: Robust and ready," *J. Field Robot.*, vol. 24, no. 6, pp. 473–485, Jun. 2007.

[12] S. Zhang, J. Yu, A. Zhang, and F. Zhang, "Spiraling motion of underwater gliders: Modeling, analysis, and experimental results," *Ocean Eng.*, vol. 60, pp. 1–13, Mar. 2013.

[13] N. E. Leonard *et al.*, "Coordinated control of an underwater glider fleet in an adaptive ocean sampling field experiment in Monterey Bay," *J. Field Robot.*, vol. 27, no. 6, pp. 718–740, 2010.

[14] X. Tan, "Autonomous robotic fish as mobile sensor platforms: Challenges and potential solutions," *Mar. Technol. Soc. J.*, vol. 45, no. 4, pp. 31–40, Jul./Aug. 2011.

[15] P. R. Bandyopadhyay, "Trends in biorobotic autonomous undersea vehicles," *IEEE J. Ocean. Eng.*, vol. 30, no. 1, pp. 109–139, Jan. 2005.

[16] V. Kopman and M. Porfiri, "Design, modeling, and characterization of a miniature robotic fish for research and education in biomimetics and bioinspiration," *IEEE/ASME Trans. Mechatron.*, vol. 18, no. 2, pp. 471–483, Apr. 2013.

[17] J. Liang, T. Wang, and L. Wen, "Development of a two-joint robotic fish for real-world exploration," *J. Field Robot.*, vol. 28, no. 1, pp. 70–79, Jan./Feb. 2011.

[18] R. Mason and J. W. Burdick, "Experiments in carangiform robotic fish locomotion," in *Proc. IEEE ICRA*, 2000, vol. 1, pp. 428–435.

[19] K. A. Morgansen, B. I. Triplett, and D. J. Klein, "Geometric methods for modeling and control of free-swimming fin-actuated underwater vehicles," *IEEE Trans. Robot.*, vol. 23, no. 6, pp. 1184–1199, Dec. 2007.

[20] Z. Chen, S. Shatara, and X. Tan, "Modeling of biomimetic robotic fish propelled by an ionic polymer-metal composite caudal fin," *IEEE/ASME Trans. Mechatron.*, vol. 15, no. 3, pp. 448–459, Jun. 2010.

[21] F. Zhang, J. Thon, C. Thon, and X. Tan, "Miniature underwater glider: Design and experimental results," *IEEE/ASME Trans. Mechatron.*, vol. 19, no. 1, pp. 394–399, Feb. 2014.

[22] F. Zhang, F. Zhang, and X. Tan, "Tail-enabled spiraling maneuver for gliding robotic fish," *J. Dyn. Syst., Meas., Control*, vol. 136, no. 4, 2014, Art ID. 041028.

[23] F. Zhang *et al.*, "Gliding robotic fish for mobile sampling of aquatic environments," in *Proc. 11th IEEE Int. Conf. Netw., Sens. Control*, Miami, FL, USA, 2014, pp. 167–172.

[24] F. Zhang and X. Tan, "Three-dimensional spiral tracking control for gliding robotic fish," in *Proc. 53rd IEEE Conf. Decis. Control*, Los Angeles, CA, USA, 2014, pp. 5340–5345.

[25] F. Zhang and X. Tan, "Gliding robotic fish and its tail-enabled yaw motion stabilization using sliding mode control," in *Proc. ASME Dyn. Syst. Control Conf.*, Palo Alto, CA, USA, 2013, Art ID. DSCC2013-4015.

[26] D. L. Rudnick, R. E. Davis, C. C. Eriksen, D. M. Fratantoni, and M. J. Perry, "Underwater gliders for ocean research," *Mar. Technol. Soc. J.*, vol. 38, no. 2, pp. 73–84, 2004.

[27] The Autonomous Underwater Vehicle Applications Center (AUVAC), "AUVs database in AUVAC." [Online]. Available: http://auvac.org/explore-database/simple-search

[28] UK National Oceanography Centre. Autosubs. [Online]. Available: http://noc.ac.uk/research-at-sea/nmfss/nmep/autosubs

[29] N. Mahmoudian, J. Geisbert, and C. Woolsey, "Approximate analytical turning conditions for underwater gliders: Implications for motion control and path planning," *IEEE J. Ocean. Eng.*, vol. 35, no. 1, pp. 131–143, Jan. 2010.

[30] J. Huisman, H. C. Matthijs, and P. M. Visser, *Harmful Cyanobacteria*. New York, NY, USA: Springer-Verlag, 2005.

[31] W. S. Davis and T. P. Simon, *Biological Assessment and Criteria: Tools for Water Resource Planning and Decision Making*. Boca Raton, FL, USA: CRC Press, 1995.

[32] G. A. Codd, L. F. Morrison, and J. S. Metcalf, "Cyanobacterial toxins: Risk management for health protection," *Toxicol. Appl. Pharmacol.*, vol. 203, no. 3, pp. 264–272, Mar. 2005.

[33] I. Chorus, I. R. Falconer, H. J. Salas, and J. Bartram, "Health risks caused by freshwater cyanobacteria in recreational waters," *J. Toxicol. Environ. Health B, Crit. Rev.*, vol. 3, no. 4, pp. 323–347, Oct.–Dec. 2000.

[34] F. M. Van Dolah, "Marine algal toxins: Origins, health effects, and their increased occurrence," *Environ. Health Perspect.*, vol. 108, no. Suppl 1, pp. 131–141, Mar. 2000.

[35] Office of Naval Research. ONR's Science of Autonomy Program. [Online]. Available: http://www.onr.navy.mil/en/Media-Center/Press-Releases/2014//media/Fil\ignorespaceses/Conferences/FAF-Autonomy/Factsheet.ashx

Feitian Zhang (S'12–M'14) received the Bachelor's and Master's degrees in automatic control from Harbin Institute of Technology, Harbin, China, in 2007 and 2009, respectively, and the Ph.D. degree in electrical and computer engineering from Michigan State University, East Lansing, MI, USA, in 2014.

He is currently a Postdoctoral Research Associate with the Department of Aerospace Engineering, University of Maryland, College Park, MD, USA. His research interests include mechatronics systems, control systems, and underwater robotics.

Osama Ennasr received the B.S. degree in electrical engineering from Michigan State University, East Lansing, MI, USA, in 2013. He is currently working toward the Ph.D. degree in the Smart Microsystems Laboratory, Michigan State University.

His research interests include cooperative control of a group of robots, embedded systems, and bioinspired underwater robots and their applications.

Elena Litchman received the B.S. degree from Moscow State University, Moscow, Russia, and the Ph.D. degree in ecology from the University of Minnesota, Minneapolis, MN, USA.

She is a Professor of aquatic ecology with the Department of Integrative Biology and Kellogg Biological Station, Michigan State University, East Lansing, MI, USA. She has published 60 peer-reviewed articles, including papers in Nature, Science and PNAS, and three book chapters. Her research interests are community ecology of plankton in freshwater and marine systems, the effects of global environmental change on aquatic ecosystems, water quality, and harmful algal blooms.

Dr. Litchman was a recipient of the National Science Foundation CAREER and PECASE Awards. She is on the Editorial Board of the *Journal of Plankton Research* and also served as an Associate Editor for *Oecologia*.

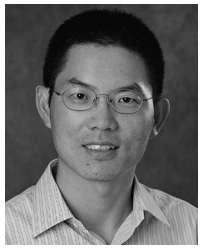

Xiaobo Tan (S'97–M'02–SM'11) received the B.Eng. and M.Eng. degrees in automatic control from Tsinghua University, Beijing, China, in 1995 and 1998, respectively, and the Ph.D. degree in electrical and computer engineering from the University of Maryland, College Park, MD, USA, in 2002.

He is currently a Professor with the Department of Electrical and Computer Engineering, Michigan State University (MSU), East Lansing, MI, USA. He has coauthored one book (Biomimetic Robotic Artificial Muscles) and over 60 peer-reviewed journal papers and holds one U.S. patent. His current research interests include modeling and control of systems with hysteresis, electroactive polymer sensors and actuators, and bioinspired underwater robots and their application to environmental sensing.

Dr. Tan currently serves as an Associate Editor/Technical Editor for *Automatica*, the IEEE/ASME TRANSACTIONS ON MECHATRONICS, and the *International Journal of Advanced Robotic Systems*. He served as the Program Chair of the 2011 International Conference on Advanced Robotics and the Finance Chair of the 2015 American Control Conference. He was a recipient of the National Science Foundation CAREER Award (2006), the MSU Teacher-Scholar Award (2010), and several Best Paper Awards.